Robust Multirate Control Scheme With Predictive Virtual Lanes for Lane-Keeping System of Autonomous Highway Driving

Young Seop Son, Wonhee Kim, *Member, IEEE*, Seung-Hi Lee, and Chung Choo Chung, *Member, IEEE*

***Abstract*—In this paper, we propose a new approach for a robust multirate lane-keeping control scheme with predictive virtual lanes. First, the multirate lane-keeping control scheme is proposed to improve the lane-keeping performance and to reduce the ripple in the yaw rate. To improve the lane-keeping performance on a curved road, the integral of the lateral offset error is added to the state feedback controller. A multirate Kalman filter (KF) has been developed to resolve the problems caused by slow lane detection due to the vision processing system. This multirate KF estimates vehicle states at a fast rate using a microprocessor. Utilizing the estimated states, the linear quadratic state feedback control operates at the same fast update rate of the microprocessor. Thus, a multirate control scheme can reduce the ripple in the yaw rate. Second, we propose a virtual lane prediction method that compensates for the momentary failure of lane detection from unexpected problems. If the camera sensor momentarily fails while obtaining lane information, the predicted virtual lane can be substituted for the lane detection using the camera sensor in the proposed control scheme. Thus, the proposed control scheme can normally operate when the lane information is momentarily unavailable. The performance of the proposed method was evaluated via experiments.**

***Index Terms*—Estimation, lane detection, lane-keeping control, multirate control.**

NOMENCLATURE

$\{XYZ\}$	Inertial coordinate frame.
$\{xyz\}$	Local coordinate frame.
x	Longitudinal position of the origin of the $\{xyz\}$ coordinate to the front fixed point.
y	Lateral position of the origin of the $\{xyz\}$ coordinate to the rotation center "O" along the lateral axis.
V	Velocity at the center of gravity (c.g.) of a vehicle.
$\dot{x} = V_x$	Longitudinal velocity at the c.g. of a vehicle.
$\dot{y} = V_y$	Lateral velocity at the c.g. of a vehicle.
m	Total mass of a vehicle.
I_z	Yaw moment of inertia of a vehicle
$l_f(l_r)$	Longitudinal distance from the c.g. to front (rear) tires.
$\dot{\psi}_d$	Desired yaw rate from the road.
ψ	Yaw, heading, and angle of a vehicle in the global axis.
$\dot{\psi} = \gamma$	Yaw rate of a vehicle.
β	Vehicle slip angle at the c.g. of a vehicle.
$\alpha(\alpha_f, \alpha_r)$	Slip angle at (front,rear) wheel tires.
δ	Steering angle.
$C_\alpha(C_{\alpha f}, C_{\alpha r})$	Cornering stiffness of (front, rear) tires.
$F_y(F_{yf}, F_{yr})$	Lateral tire force (on front and rear tires).
R	Turn radius of a vehicle or radius of the road.
$\rho = 1/R$	Curvature of the road.
L	Look-ahead distance from the c.g. to the look-ahead point.
$e_y = y - y_d$	Lateral position error with respect to the reference.
$e_\psi = \psi_d - \psi$	Yaw angle error with respect to the road.

PARAMETER DEFINITIONS

$$a_{22} = -\frac{2C_{\alpha f} + 2C_{\alpha r}}{mV_x}, \quad a_{23} = -a_{22}V_x$$

$$a_{24} = -\frac{2C_{\alpha f}l_f - 2C_{\alpha r}l_r}{mV_x}, \quad a_{42} = -\frac{2C_{\alpha f}l_f - 2C_{\alpha r}l_r}{I_zV_x}$$

$$a_{43} = -a_{42}V_x, \quad a_{44} = -\frac{2C_{\alpha f}l_f^2 + 2C_{\alpha r}l_r^2}{I_zV_x}$$

$$b_{21} = \frac{2C_{\alpha f}}{mV_x}, \quad b_{41} = \frac{2C_{\alpha f}l_f}{I_z}.$$

Manuscript received September 25, 2013; revised January 29, 2014 and May 16, 2014; accepted August 18, 2014. Date of publication September 8, 2014; date of current version August 11, 2015. This work was supported by the Ministry of Trade, Industry, and Energy of Korea through the Industrial Strategic Technology Development Program under Grant 10042808 (Development of Driver Assistance Systems Using Camera, Radar and Road Characteristics) and Grant 10044620 (Automatic Lane Change System for Novice Drivers). The review of this paper was coordinated by Prof. J. Wang.

Y. S. Son is with the Department of Electrical Engineering, Hanyang University, Seoul 133-791, Korea, and also with Global R&D Center, MANDO Corporation, Seongnam 463-400, Korea (e-mail: youngseop.son@halla.com).

W. Kim is with the Department of Electrical Engineering, Dong-A University, Busan 604-714, Korea (e-mail: whkim79@dau.ac.kr).

S.-H. Lee and C. C. Chung are with the Division of Electrical and Biomedical Engineering, Hanyang University, Seoul 133-791, Korea (e-mail: shlee@ieee.org; cchung@hanyang.ac.kr).

Color versions of one or more of the figures in this paper are available online at http://ieeexplore.ieee.org.

Digital Object Identifier 10.1109/TVT.2014.2356204

I. INTRODUCTION

AUTONOMOUS highway driving has become an important issue in the automotive industry. More than 90% of

highway accidents are caused by human error [1]. Autonomous vehicles are expected to enhance driving safety and to reduce the driver's workload so that they can reduce accidents on the highway. From the mid-1980s to the mid-1990s, due to the technological limitations of sensors, microprocessors, and communications, most studies relied on buried magnets or electrified wires placed along the path for the detection of the vehicle lateral position; this is the so-called infrastructure-based approach. In the Partners for an Advanced Transit and Highways (PATH) program, an infrastructure-based approach was investigated based on a reference/sensing highway system [2]. For sensing lanes on the highway, this method used discrete magnetic markers embedded in the roadway, forming a predetermined path, and a magnetometer mounted in front of the experimental vehicles [2]–[5]. Due to limitations of the sensing system, these methods were designed based on a look-down sensing scheme. The fundamental control difficulties of this approach were presented in [6]. Furthermore, modification of the infrastructure by burying the sensors in the roadway would be time-consuming and costly.

With the development of technology, it has become ever more common for vision-based algorithms to avoid the modification of infrastructures and to find application in real-time control tasks. A vision sensor can detect look-ahead distance, giving us the look-ahead sensing scheme introduced in [7]. It was reported that the state in terms of the lateral error at the look-ahead distance improves the performance of lane-keeping control [8]. A lane-keeping control method using the images obtained from a charge-coupled device camera mounted in the vehicle was presented in [9]. In [10], an intelligent automated lane-keeping system was proposed and implemented on their vehicle platform. Cerone *et al.* addressed the problem of combining automatic lane-keeping and driver's steering for obstacle avoidance and lane-change maneuvers for passing purposes through a closed-loop control strategy [11]. A lane-keeping control method using a potential field was designed to solve the stability and robustness issues for a simple look-ahead control scheme [12]. A model predictive control having dual prediction horizons was proposed to reduce the length of the prediction horizon and rapidly obtain an optimal solution [13]. Although the previous methods improved the lane-keeping performance, only the lateral offset error at the look-ahead distance was used in the control methods. This may result in increasing the offset error due to the disturbance on a curved road.

A camera sensor is widely used to obtain lane information due to its low cost relative to other lane detection sensors for lane-keeping controls [7]–[13]. Various detection methods have been studied to obtain the lane information using camera sensors [14]–[16]. When the camera sensor is used in an autonomous vehicle system, two main problems occur. First, when the camera sensor is used with microprocessors and other sensors, e.g., an inertial measurement unit (IMU) sensor, the overall system for autonomous vehicles becomes a multirate system due to the their different sampling rates. To obtain the control input for lane-keeping, the road information should first be obtained by the camera sensor. However, the camera sensor has a relatively slow update time compared with those of the microprocessors and other sensors. The problem of a slow update rate and the time delay of vision processing systems causes inaccurate control and undesirable lateral behavior, such as oscillatory responses due to the loss of damping [17]. Furthermore, intersample ripples in the multirate system may occur in the closed-loop system due to the control chattering [18]–[20]. In particular, the ripple in the yaw rate is the main cause of an uncomfortable feeling for the driver [21]. Nonetheless, in the previous lane-keeping control approaches, their control algorithms operated at the same slow rate of vision processing. The second problem is that both weather and environment strongly influence the performance of lane detection based on camera sensors [22]. Therefore, in the past few years, various approaches for lane detection have been proposed and have successfully demonstrated their robustness in environments [23]–[28]. Although these previous approaches are effective at detecting a lane, they can be used only when the camera sensor operates normally. Therefore, when lane information from a camera sensor is unavailable due to unexpected problems, (e.g., complex shadowing, poor lane markings, complex characters, lighting changes, different lane intensities, and/or malfunction of the camera sensor) the previous approaches cannot be used.

In this paper, we propose a new approach for a robust multirate lane-keeping control scheme with a predictive virtual lane to overcome the aforementioned problems for a lane-keeping system. First, the multirate lane-keeping control scheme is proposed to improve the lane-keeping performance and to reduce the ripple in the yaw rate. To improve the lane-keeping performance on a curved road, we develop a linear quadratic state feedback control using both the lateral offset error at the look-ahead distance and the integral of the look-down lateral offset error. The multirate Kalman filter (KF) is developed to resolve the aforementioned problems occurring due to slow lane detection by the vision processing system. Using the data measured from the camera sensor at a slow rate, this multirate KF estimates the vehicle states at a fast rate of the microprocessor. Utilizing the estimated states, the linear quadratic state feedback control operates at the same fast update rate of the engine control unit. Thus, a multirate control scheme can reduce the ripple in the yaw rate. Second, we propose a virtual lane prediction method to cope with the momentary failure of lane detection from unexpected problems (e.g., complex shadowing, poor lane markings, complex characters, lighting changes, different lane intensities and/or malfunction of the camera sensor, etc.) To predict the lane, the third polynomial function of the longitudinal distance is used as the lane model [29], [30]. Each coefficient of the lane polynomial function at the next sampling time is geometrically calculated by using the relative movements of the vehicle and lanes and the longitudinal velocity and the yaw of vehicle at present. Then, the predictive virtual lane at the next sampling time is obtained without the lane information from the camera sensor at the next sampling time. When obtaining lane information from a camera sensor has a momentary failure, the virtual lane predicted from a previous sampling time can be substituted for lane detected by using the camera sensor in the proposed control scheme. Thus, the proposed control scheme can normally operate when the lane information is momentarily unavailable.

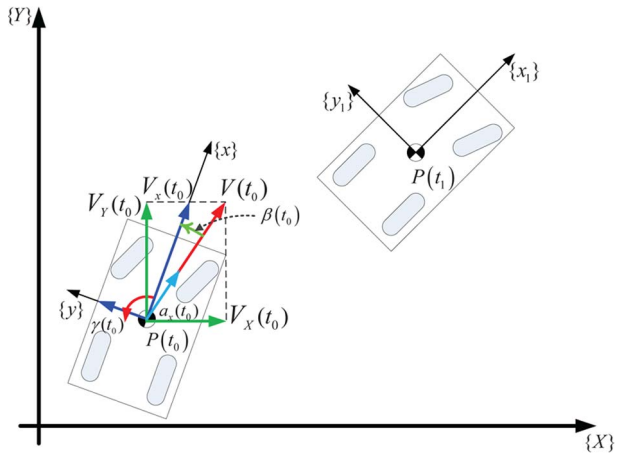

Fig. 1. Kinematic motion of vehicle.

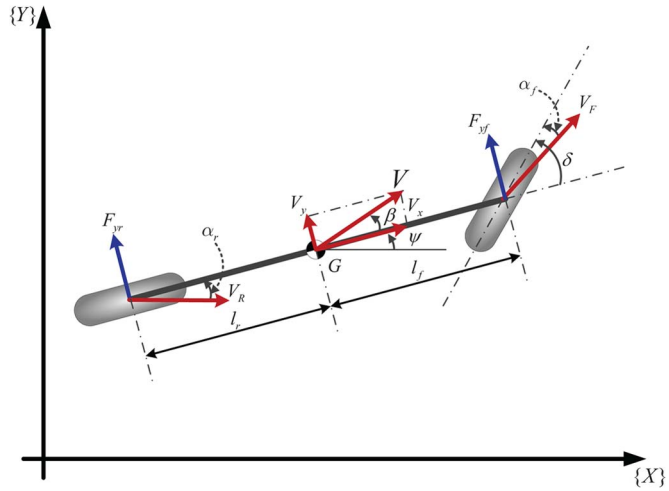

Fig. 2. Bicycle model diagram of lateral vehicle dynamics.

The performance of the proposed method was evaluated via experiments. The contributions of this paper are summarized as follows.

1) The multirate KF estimates vehicle states at the fast rate of the microprocessor so that the control algorithm can be operated at a fast rate.
2) The linear quadratic state feedback control using both the lateral offset error at the look-ahead distance and the integral of the look-down lateral offset error improves the lane-keeping performance on a curved road.
3) Multirate control scheme reduces the ripple in the yaw rate.
4) The predictive virtual lane method allows the proposed control scheme to operate normally when the lane information is momentarily unavailable.

II. Vehicle Lateral Dynamics Modeling and Lane Modeling

A. Vehicle Kinematics Modeling

We assume that a vehicle has planar motion, as shown in Fig. 1. To describe the motion of the vehicle, we use three degrees of freedom (DOFs): longitudinal x, lateral y, and yaw ψ. $\{X\}$ and $\{Y\}$ are global coordinates of the location of the c.g. of the vehicle, whereas $\{x\}$ and $\{y\}$ are the local coordinates in the viewpoint of the c.g. of the vehicle at time t_0. In Fig. 1, $\{x_1\}$ and $\{y_1\}$ are the new local coordinates in the viewpoint of the c.g. of the vehicle at time t_1. ψ is the orientation angle of the vehicle with respect to the axis. V is the velocity of the vehicle, and V_X and V_Y are the vehicle velocities of the X-axis and Y-axis, respectively. V_x is the longitudinal velocity of the vehicle, a_x is the longitudinal acceleration, γ is the yaw rate, and β is the sideslip angle. If the vehicle has momentum of motion at the initial position $P(t_0) = [X(t_0), Y(t_0), \psi(t_0)]^T$ with $V_x(t_0)$, $a_x(t_0)$, $\gamma(t_0)$, and $\beta(t_0)$, the velocity of the vehicle at time t_1 in the plane at point $P(t_1)$ is

$$V(t_1) = V(t_0) + \int_{t_0}^{t_1} a_x(\tau)\, d\tau$$

$$\psi(t_1) = \psi(t_0) + \int_{t_0}^{t_1} \gamma(\tau)\, d\tau. \tag{1}$$

Then, V_X and V_Y at time t_1 are given by

$$\begin{aligned} V_X(t_1) &= V(t_1)\cos\left(\psi(t_1) - \beta(t_1)\right) \\ V_Y(t_1) &= V(t_1)\sin\left(\psi(t_1) - \beta(t_1)\right). \end{aligned} \tag{2}$$

Finally, we can obtain the global position of the vehicle at time t_1, i.e., $P(t_1) = [X(t_1), Y(t_1), \psi(t_1)]^T$, as follows:

$$P(t_1) = \begin{bmatrix} X(t_1) \\ Y(t_1) \\ \psi(t_1) \end{bmatrix} = \begin{bmatrix} X(t_0) + \int_{t_0}^{t_1} V_X(\tau)\, d\tau \\ Y(t_0) + \int_{t_0}^{t_1} V_Y(\tau)\, d\tau \\ \psi(t_0) + \int_{t_0}^{t_1} \gamma(\tau)\, d\tau \end{bmatrix}. \tag{3}$$

B. Vehicle Lateral Dynamics Modeling

The detailed dynamics of a vehicle including the longitudinal and the lateral dynamics can be described with a mechanical model that naturally has a minimum of six DOFs [31]. In this paper, we assume a high-level longitudinal velocity controller working such that the vehicle longitudinal velocity V_x settles to a given longitudinal velocity command in a finite amount of time [4], [9], [29], [32], [33]. The bicycle model, as shown in Fig. 2, is used for lateral vehicle dynamics. The lateral position error, lateral position error at the look-ahead distance point, heading angle, and reference trajectory are described in Fig. 3. We define the vehicle lateral states $\mathbf{x}$ as

$$\mathbf{x} = \begin{bmatrix} e_{yL_e} \\ \dot{e}_y \\ e_\psi \\ \dot{\psi} \end{bmatrix} = \begin{bmatrix} (y - y_d) + L(\psi - \psi_d) \\ \dot{y} - \dot{y}_d \\ \psi - \psi_d \\ \dot{\psi} \end{bmatrix} \tag{4}$$

where y_d is the desired lateral offset error, and ψ_d is the desired yaw. Let us describe the basic lateral model in terms of the lateral offset at the vehicle's c.g. and convert it in terms of

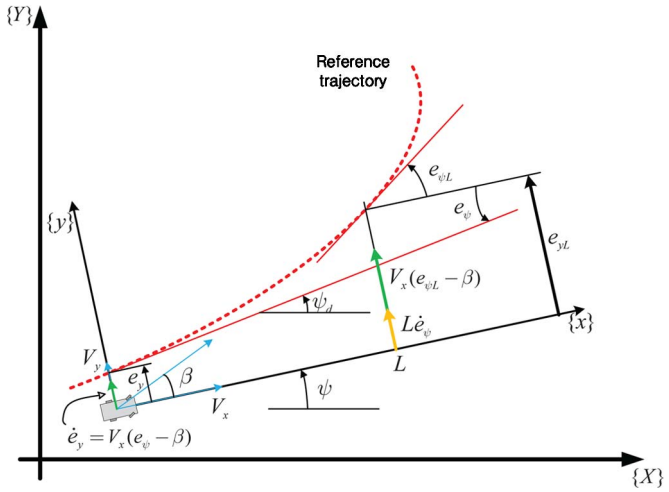

Fig. 3. Lateral position and velocity errors at the look-ahead distance point.

the lateral offset at the look-ahead distance. The vehicle lateral dynamics in terms of the state vector are then obtained by

$$\dot{\mathbf{x}} = \underbrace{\begin{bmatrix} 0 & 1 & 0 & L \\ 0 & a_{22} & a_{23} & a_{24} \\ 0 & 0 & 0 & 1 \\ 0 & a_{42} & a_{43} & a_{44} \end{bmatrix}}_{A} \mathbf{x} + \underbrace{\begin{bmatrix} 0 \\ b_{21} \\ 0 \\ b_{41} \end{bmatrix}}_{B} u + \underbrace{\begin{bmatrix} -L \\ -V_x \\ -1 \\ 0 \end{bmatrix}}_{B_{\psi}} \dot{\psi}_d. \quad (5)$$

The detailed mathematical modeling is discussed in [31], [34], and [35].

C. Lane and Vehicle Trajectory Modeling

The camera sensor detects the lane based on the local coordinate of the vehicle. Thus, from now on, vehicle trajectory $f_v(x)$ and lane polynomials $f_L(x)$ and $f_R(x)$ will be described based on the local coordinate of the vehicle $\{x\}$ and $\{y\}$. Fig. 4 shows the information of a lane detected by the camera sensor toward the longitudinal direction and a vehicle's trajectory. The vehicle trajectory $f_v(x)$ is obtained using parabolic projection with arc approximation under the assumption that it moves at a constant speed V_x and at a constant yaw rate $\dot{\psi}$ [31], [36], [37] as follows:

$$f_v(x) = \frac{\rho_v}{2}x^2 = \frac{\dot{\psi}}{2V_x}x^2 \quad (6)$$

where ρ_v is the curvature of a circular road, and x is the longitudinal distance. From the information of a lane detected by the camera sensor toward the longitudinal direction, left- and right-lane polynomials $f_L(x)$ and $f_R(x)$ are defined as the third-order polynomial functions of the longitudinal distance x [23], [24], [29], [30], [38] such that

$$\begin{aligned} f_L(x) &= c_{L_0} + c_{L_1}\cdot x + c_{L_2}\cdot x^2 + c_{L_3}\cdot x^3 \\ f_R(x) &= c_{R_0} + c_{R_1}\cdot x + c_{R_2}\cdot x^2 + c_{R_3}\cdot x^3 \end{aligned} \quad (7)$$

where c_{L_0} and c_{R_0} represent the lateral offsets, c_{L_1} and c_{R_1} are the head angles, c_{L_2} and c_{R_2} are the curvature, and c_{L_3} and c_{R_3} are the curvature rates of the left and right lanes, respectively.

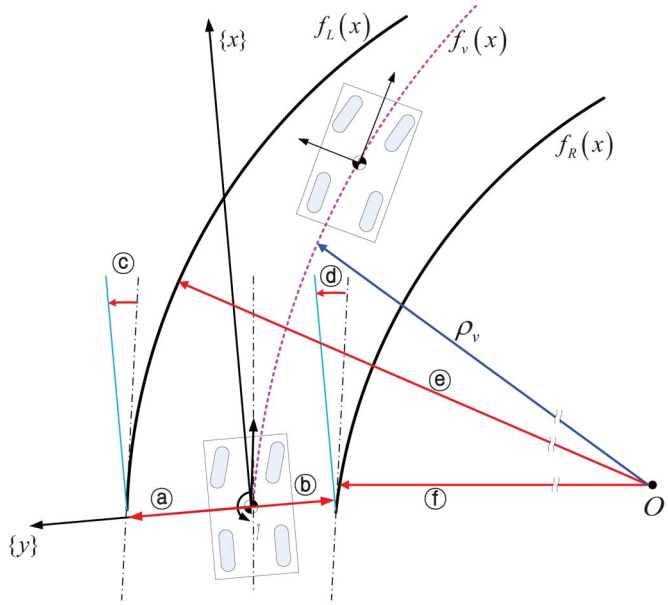

Symbols	Definition
ⓐ,ⓑ	Left and right lateral offsets
ⓒ,ⓓ	Left and right heading angles
ⓔ,ⓕ	Left and right curvatures & derivatives

Fig. 4. Trajectories of lane and vehicle.

Then, the desired lane polynomial of the vehicle is obtained by taking the average of $f_L(x)$ and $f_R(x)$ such that

$$f_d(x) = c_0 + c_1\cdot x + c_2\cdot x^2 + c_3\cdot x^3 \quad (8)$$

where $c_0 = (c_{L_0} + c_{R_0})/2$ is the lateral offset, $c_1 = (c_{L_1} + c_{R_1})/2$ is the head angle, $c_2 = (c_{L_2} + c_{R_2})/2$ is the curvature, and $c_3 = (c_{L_3} + c_{R_3})/2$ is the curvature rate. The lane polynomial is fixed until the lane information arrives at the next interval, but the vehicle's trajectory is determined by the vehicle's momentum such as velocity and yaw rate.

III. Multirate Lane-Keeping Control System

A. Lane-Keeping Controller

From (6), we obtain the desired lateral offset at the look-ahead distance e_{yL_d} and the desired yaw rate $\dot{\psi}_d$ as

$$e_{yL_d} = \frac{\rho_v}{2}x^2 = \frac{\dot{\psi}}{2V_x}x^2 \quad (9)$$

$$\dot{\psi}_d = \frac{V_x}{R} = 2c_2V_x. \quad (10)$$

The control that aims to make the vehicle maintain the reference trajectory are as follows:

$$\begin{aligned} \lim_{t\to\infty} e_{yL} &= e_{yL_d} \\ \lim_{t\to\infty} \dot{e}_y &= 0 \\ \lim_{t\to\infty} e_{\psi} &= 0 \\ \lim_{t\to\infty} \dot{\psi} &= \dot{\psi}_d. \end{aligned} \quad (11)$$

The error is defined as

$$\mathbf{e} = \begin{bmatrix} e_{yLe_I} \\ e_{yL_e} \\ \dot{e}_y \\ e_\psi \\ \dot{e}_\psi \end{bmatrix} = \begin{bmatrix} \int_0^t e_{yLe} d\tau \\ e_{yL} - e_{yL_d} \\ \dot{y} - \dot{y}_d \\ \psi - \psi_d \\ \dot{\psi} - \dot{\psi}_d \end{bmatrix}. \tag{12}$$

From (5) and (12), we have the error dynamics as

$$\begin{aligned} \dot{\mathbf{e}} = & \underbrace{\begin{bmatrix} 0 & 1 & 0 & 0 & 0 \\ 0 & 0 & 1 & 0 & L \\ 0 & 0 & a_{22} & a_{23} & a_{24} \\ 0 & 0 & 0 & 0 & 1 \\ 0 & 0 & a_{42} & a_{43} & a_{44} \end{bmatrix}}_{A_e} \mathbf{e} + \underbrace{\begin{bmatrix} 0 \\ 0 \\ b_{21} \\ 0 \\ b_{41} \end{bmatrix}}_{B_e} u \\ & + \underbrace{\begin{bmatrix} 0 & 0 \\ -1 & -L \\ 0 & -V_x + a_{24} \\ 0 & 0 \\ 0 & a_{44} \end{bmatrix}}_{B_w} \underbrace{\begin{bmatrix} \dot{e}_{yL_d} \\ \dot{\psi}_d \end{bmatrix}}_{\mathbf{w}} \\ \mathbf{y_e} = & \underbrace{\begin{bmatrix} 1 & 0 & 0 & 0 & 0 \\ 0 & 1 & 0 & 0 & 0 \\ 0 & 0 & 0 & 1 & 0 \\ 0 & 0 & 0 & 0 & 1 \end{bmatrix}}_{C_e} \mathbf{e}. \end{aligned} \tag{13}$$

Since we assumed that V_x is constant, $\ddot{\psi}_d$ becomes zero from (10) [31]. We can regard $\mathbf{w}$ as a disturbance vector from the viewpoint of the regulation of $\mathbf{e}$. On a straight road, $\mathbf{w}$ is almost zero. In contrast, $\mathbf{w}$ disturbs the lane keeping since $\mathbf{w}$ is not zero on a curved road. Thus, the integrator is added to the controller to suppress any steady-state error due to the disturbances $\mathbf{w}$ in $\mathbf{e}$. The linear system (13) is parameterized with the longitudinal velocity V_x and look-ahead distance L. Fig. 5 shows the root locus of the error dynamics (13). The root locus for $L = 10$ m, $L = 15$ m, and $L = 20$ m, with $V_x = 100$ km/h, is shown in Fig. 5(a). As shown in Fig. 5(a), given the variation of L, the system remains stable. However, the variation of L affects the locations of the zeros such that the damping ratio of the dominant poles is influenced. As L is close to the front of the vehicle, the damping ratio of the poles in (13) drastically declines. A high-gain controller moves the closed-loop poles toward the zeros, resulting in a poorly damped closed-loop system. Thus, a longer look-ahead distance is better than the shorter look-ahead distance. However, L cannot be chosen to be very distant from the vision system due to the performance of the vision system. From many experimental verifications, we chose the value of L equal to 20 m. The root locus for $V_x = 100$ km/h, $V_x = 130$ km/h, and $V_x = 160$ km/h with $L = 20$ m is shown in Fig. 5(b). It is observed that the variation of V_x affected both the poles and the zeros. Increasing V_x moves both the poles and zeros toward the imaginary axis. Thus, the stability can be affected by the variation of V_x. Furthermore, the zero is moved toward the imaginary axis so that the damping ratio of the poles in (13) drastically declines in the high-gain controller to regulate $\mathbf{e}$, the state feedback control is used as

$$u(t) = -K_c \mathbf{e}(t) \tag{14}$$

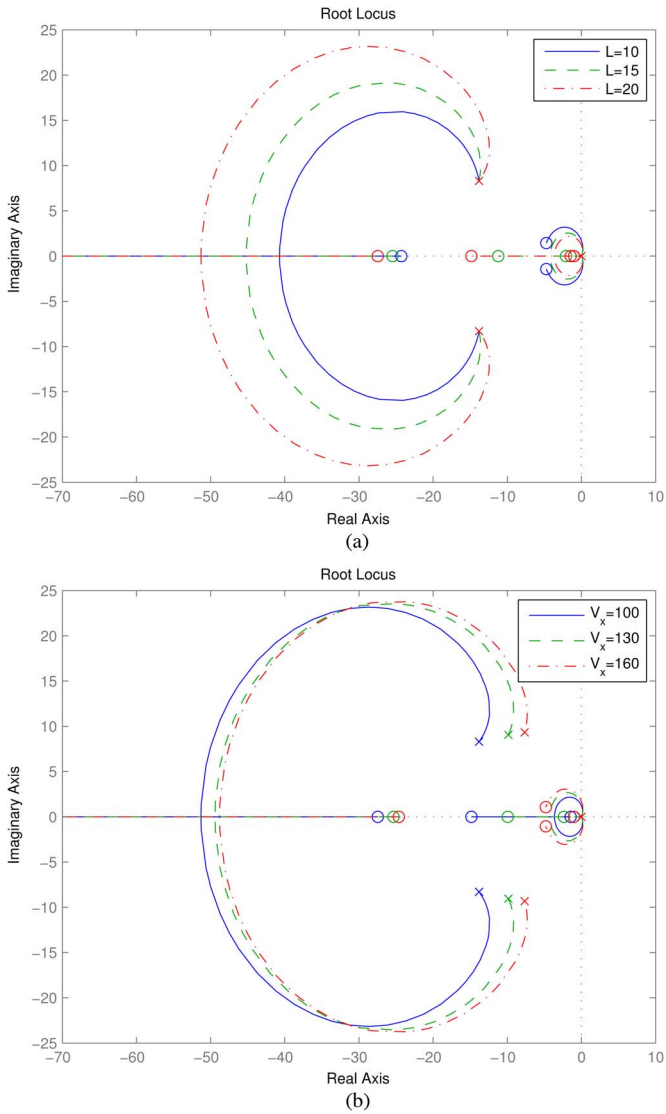

Fig. 5. Root locus of the error dynamics (13). (a) For $L = 10$ m, $L = 15$ m, and $L = 20$ m with $V_x = 100$ km/h. (b) For $V_x = 100$ km/h, $V_x = 130$ km/h, and $V_x = 160$ km/h with $L = 20$ m.

where the optimal state feedback gain K_c can be obtained by solving the Riccati equation to minimize the linear quadratic cost as follows:

$$J_c = \int_0^t \mathbf{e}^T(\tau) R_{e_c} \mathbf{e}(\tau) + u^T(\tau) R_{u_c} u(\tau)\, d\tau \tag{15}$$

where R_{e_c} and R_{u_c} are weighted matrices. The effect of the disturbance $\mathbf{w}$ to the lane-keeping performance can be suppressed by the integrator term. This will be shown in Section V. It is also possible to apply predictive control, which has recently been increasing in popularity. Some predictive control techniques developed for fast real-time applications are useful for automotive motion control [41].

B. Multirate State Estimation

Fig. 6 shows the block diagram of the lateral lane-keeping control system. The yaw rate $\dot{\psi}$ is measured by the IMU sensor.

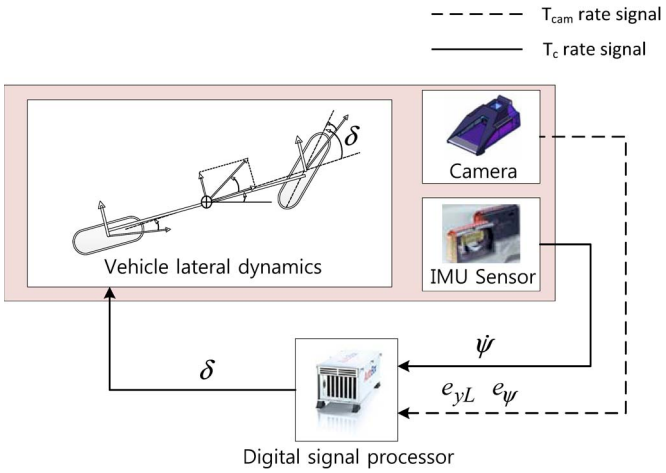

Fig. 6. Block diagram of the lateral keeping control system.

The lateral offset at the look-ahead distance e_{yL} and yaw angle error e_ψ are measured by the camera. In Fig. 6, T_c is the control update period, and $T_{\rm cam}$ is the update period of the vision processing system. Without loss of generality, we assume that $T_{\rm cam}$ is chosen such that it can be represented as $T_{\rm cam} = R_m T_c$ for some integers $R_m \geq 1$. Then, we can represent a time instant

$$t = \left(k + \frac{i}{R_m}\right) T_{\rm cam} \tag{16}$$

for $k = 0, 1, \ldots$ and $i = 0, 1, \ldots, R_m - 1$. Here, the indexes k and i indicate the vision processing update and the control update instants, respectively. In the interim, the microprocessor is operating at a rate of $1/T_c$.

1) Multirate Sensing: Some measurements, such as the vehicle's yaw rate and speed, are measurable and available from the microprocessor at a sampling rate of $1/T_c$. On the other hand, the camera and vision processing system provide a lane curvature equation at the slow sampling rate of $1/T_{\rm cam}$ [38], [39]. For convenience of notation, let us partition the state vector as $\mathbf{x} = [\,\mathbf{x_s} \quad x_f\,]^T$ such that

$$\mathbf{x_s} = [\,e_{yL} \quad \dot{e}_y \quad e_\psi\,]^T, \quad x_f = \dot{\psi} \tag{17}$$

represent the states associated with the fast and slow output measurements, respectively. Then, we let

$$\mathbf{y} = \begin{bmatrix} y_s \\ y_f \end{bmatrix} = C\mathbf{x} = \operatorname{diag}(C_s, C_f) \begin{bmatrix} \mathbf{x_s} \\ x_f \end{bmatrix}. \tag{18}$$

2) Partitioned Lateral Dynamics Models: The vehicle lateral dynamics (5) can be partitioned. In regard to the state $\mathbf{x_s}$ associated with the slow vision processing measurement, the dynamics of $\mathbf{x_s}$ are given by

$$\dot{\mathbf{x}}_\mathbf{s} = \underbrace{\begin{bmatrix} 0 & 1 & 0 \\ 0 & a_{22} & a_{23} \\ 0 & 0 & 0 \end{bmatrix}}_{A_s} \mathbf{x_s} + \underbrace{\begin{bmatrix} 0 \\ b_{21} \\ 0 \end{bmatrix}}_{B_{s_u}} u + \underbrace{\begin{bmatrix} L \\ a_{24} \\ 1 \end{bmatrix}}_{A_{s_f}} x_f + \underbrace{\begin{bmatrix} L \\ V_x \\ 1 \end{bmatrix}}_{B_{\psi_s}} \dot{\psi}_d. \tag{19}$$

With regard to the state x_f describing the vehicle motion in terms of the fast rate measurements, we have

$$\dot{x}_f = \underbrace{a_{44}}_{A_f} x_f + \underbrace{b_{41}}_{B_{f_u}} u + \underbrace{\begin{bmatrix} 0 \\ a_{42} \\ a_{43} \end{bmatrix}}_{A_{f_s}} \mathbf{x_s}. \tag{20}$$

For the sampling period T_c, one can obtain the zero-order-hold (ZOH) discrete-time equivalent doublet, i.e.,

$$\left(\begin{bmatrix} \Phi_s & \Phi_{s_f} \\ \Phi_{f_s} & \Phi_f \end{bmatrix}, \begin{bmatrix} \Gamma_{s_u} & \Gamma_{\psi_s} \\ \Gamma_{f_u} & 0 \end{bmatrix} \right) \tag{21}$$

to

$$\left(\begin{bmatrix} A_s & A_{s_f} \\ A_{f_s} & A_f \end{bmatrix}, \begin{bmatrix} B_{s_u} & B_{\psi_s} \\ B_{f_u} & 0 \end{bmatrix} \right). \tag{22}$$

3) Decentralized Multirate State Estimator: The KF equations can now be completely decentralized. Each sensing implements its own local KF, arrives at a partial decision, and transfers it to the other. The state estimators for yaw rate and the longitudinal dynamics are quite typical and can be easily designed [17] and combined to estimate the state x_f at a fast rate of $1/T_c$.

The yaw rate $\dot{\psi}$ is measured by the IMU sensor at a fast rate of $1/T_c$. In contrast, lane detection from the camera vision and processing system is updated so that the lateral offset at the look-ahead distance e_{yL} and the yaw angle error e_ψ are measured at a slow rate of $1/T_{\rm cam}$. Lane detection is available at a slow rate of $1/T_{\rm cam}$, although state $\mathbf{x_s}$ needs to be estimated at a fast rate of $1/T_c$ for control algorithm implementation. We thus need to design a multirate state estimator for the lateral dynamics to estimate state x_s at a fast rate of $1/T_c$ using lane detection at a slow rate of $1/T_{\rm cam}$.

Designing a state estimator to estimate x_f is straightforward. In this case, $\hat{x}_s$ is the estimation of x_s by the multirate state estimator that will be designed. Thus

$$\begin{aligned} \bar{x}_f(k, i+1) &= \Phi_f \hat{x}_f(k,i) + \Gamma_{f_u} u(k,i) + \Phi_{f_s} \hat{\mathbf{x}}_\mathbf{s}(k,i) \\ \hat{x}_f(k,i) &= \bar{x}_f(k,i) + L_f \left(y_f(k,i) - C_f \bar{x}_f(k,i)\right) \end{aligned} \tag{23}$$

where L_f is the state estimator gain to be determined. On the other hand, to estimate the state $\mathbf{x_s}$, we should utilize the multirate estimation scheme [20] to develop

$$\begin{aligned} \bar{\mathbf{x}}_\mathbf{s}(k, i+1) &= \Phi_s \hat{\mathbf{x}}_\mathbf{s}(k,i) + \Gamma_{s_u} u(k,i) + \Phi_{s_f} \hat{\mathbf{x}}_\mathbf{f}(k,i) + \Gamma_{\psi_s} \dot{\psi}_d \\ \hat{\mathbf{x}}_\mathbf{s}(k,i) &= \bar{\mathbf{x}}_\mathbf{s}(k,i) + L_s \left(y_f(k,i) - C_s \bar{x}_s(k,i)\right) \end{aligned} \tag{24}$$

where L_s is the state estimator gain to be determined. Applying a discrete-time lifting leads to a lifted model, where

$$\bar{\mathbf{x}}_\mathbf{s}(k+1, 0) = \left(\Phi_s^{R_m} - \sum_{j=1}^{R_m} \Phi_s^j L_s C_s \right) \bar{\mathbf{x}}_\mathbf{s}(k, 0) + \cdots. \tag{25}$$

L_s is determined to make $\Phi_s^{R_m} - \Phi_s^{R_m} \tilde{L}_s C_s$, where

$$\tilde{L}_s = \Phi_s^{-R_m} \sum_{j=1}^{R_m} \Phi_s^j L_s \tag{26}$$

become stable. The state estimators (23) and (24) provide state estimates $[\mathbf{x_s} \quad x_f]$ at each microprocessor sampling period $1/T_c$.

C. Multirate Linear Quadratic Regulator Control

To use the estimated states from the multirate KF (23) and (24) for the sampling period T_c in the error dynamics (13), (A_e, B_e) is discretized using the ZOH as (Φ_e, Γ_e). Since the error $\mathbf{e}$ is obtained using estimated states from the multirate KF (23) and (24), the estimated error $\hat{\mathbf{e}}$ in discrete time is defined as

$$\hat{\mathbf{e}} = \begin{bmatrix} \hat{e}_{yLe_I} \\ \hat{e}_{yLe_e} \\ \dot{\hat{e}}_y \\ e_\psi \\ \dot{\hat{e}}_\psi \end{bmatrix} = \begin{bmatrix} \sum_0^\infty \hat{e}_{yL_e} \\ \hat{e}_{yL} - e_{yL_d} \\ \dot{\hat{e}}_y \\ e_\psi \\ \dot{\hat{\psi}} - \dot{\psi}_d \end{bmatrix}. \tag{27}$$

For regulating $\mathbf{e}$, the control law is designed as

$$u(k,i) = -K_d \hat{\mathbf{e}}(k,i) \tag{28}$$

where the optimal state feedback gain K_d can be obtained by solving the Riccati equation to minimize the linear quadratic cost in the discrete time as follows:

$$J_d = \sum_0^\infty \hat{\mathbf{e}}^T R_{e_d} \hat{\mathbf{e}} + u^T R_{u_d} u \tag{29}$$

where R_{e_d} and R_{u_d} are the weighted matrices. Utilizing the estimated states, the linear quadratic state feedback control can operate at the same fast update rate of the ECU. The effect of the multirate control to the lane-keeping performance will be shown in Section V.

IV. Virtual Lane Prediction System

The multirate lateral lane-keeping control system designed in Section III requires the lane information from the camera. When there is a failure in obtaining lane information from a camera sensor due to unexpected problems, the proposed control system may malfunction. Here, we will design a virtual lane prediction method using vehicle kinematic motion, vehicle trajectory, and lane polynomial function to avoid the momentary failure of lane detection from unexpected problems.

A. Predictive Virtual Lane

The reliable lane information is obtained from the camera at time k, and the longitudinal velocity V_x and the yaw rate γ is always measured with the same sampling rate of control. Let us assume that the position of the vehicle at time k is $[x(k, 0), y(k,0), \psi(k,0)]^T = [0,0,0]^T$. Then, the estimated position of the vehicle $[\hat{x}(k+1,0), \hat{y}(k+1,0), \hat{\psi}(k+1,0)]^T$ at time $k+1$ can be approximated via the Euler method such that

$$\hat{\psi}(k,i) = \sum_{j=0}^{i} \gamma(k,j) T_c$$

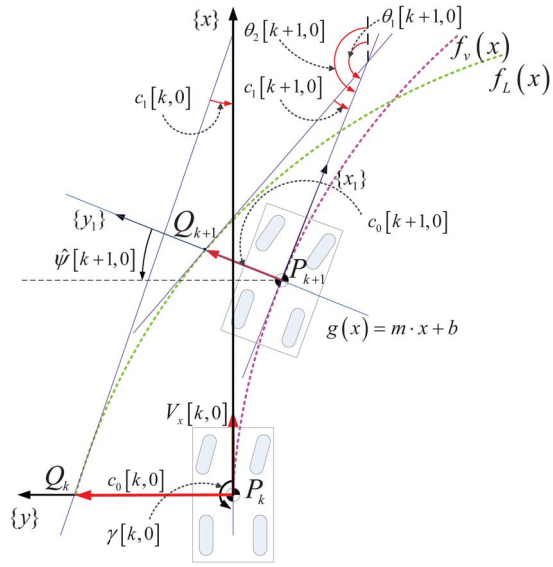

Fig. 7. Relationship between the vehicle's trajectory and lane polynomial.

Fig. 8. Test vehicle.

Fig. 9. High Speed Circuit of KATRI.

$$\hat{x}(k+1,0) = \sum_{i=0}^{R_{mv}-1} V_x(k,i) \cos\left(\hat{\psi}(k,i)\right) T_c$$
$$\hat{y}(k+1,0) = \sum_{i=0}^{R_{mv}-1} V_x(k,i) \sin\left(\hat{\psi}(k,i)\right) T_c. \tag{30}$$

Now, we can derive the prediction method to estimate the coefficients of the lane at time $k+1$.

1) Lateral Offset Estimation $\hat{c}_0$: Fig. 7 shows the relationship between the vehicle's trajectory and lane polynomial. In Fig. 7, point P_k and the angle $((\pi/2)+\hat{\psi}(k+1,0))$, which is

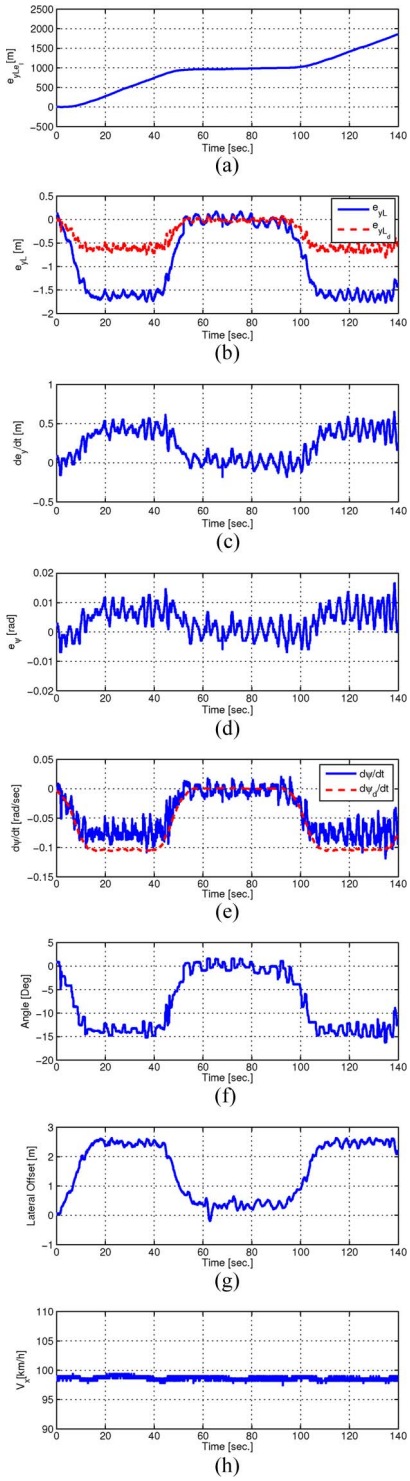

Fig. 10. Lane-keeping control performance of A.1 (single rate and without an integrator). (a) e_{yLe_I}. (b) e_{yL} and e_{yL_d}. (c) $\dot{e}_y$. (d) e_ψ. (e) $\dot{\psi}$ and $\dot{\psi}_d$. (f) Steering wheel angle. (g) e_y. (h) V_x.

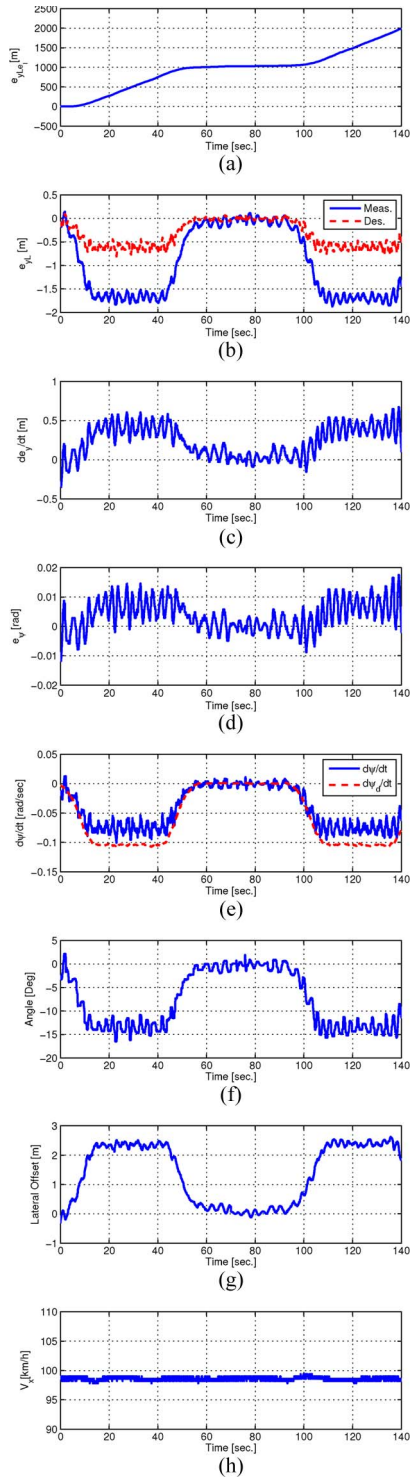

Fig. 11. Lane-keeping control performance of case A.2 (multirate and without an integrator). (a) e_{yLe_I}. (b) e_{yL} and e_{yL_d}. (c) $\dot{e}_y$. (d) e_ψ. (e) $\dot{\psi}$ and $\dot{\psi}_d$. (f) Steering wheel angle. (g) e_y. (h) V_x.

between $\overline{P_{k+1}Q_{k+1}}$ and the horizontal line, create a straight line $g(x)$ passing through both points P_{k+1} and Q_{k+1} as follows:

$$g(x) = mx + b \tag{31}$$

where $m = \tan((\pi/2) + \hat{\psi}(k+1,0))$, and $b = \hat{y}(k+1,0) - m \times \hat{x}(k+1,0)$. From (7) and (31), the intersection between

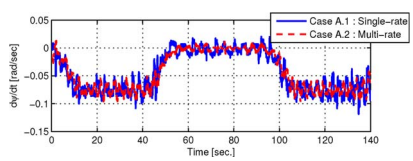

Fig. 12. Yaw rates $\dot{\psi}$ of cases A.1 and A.2.

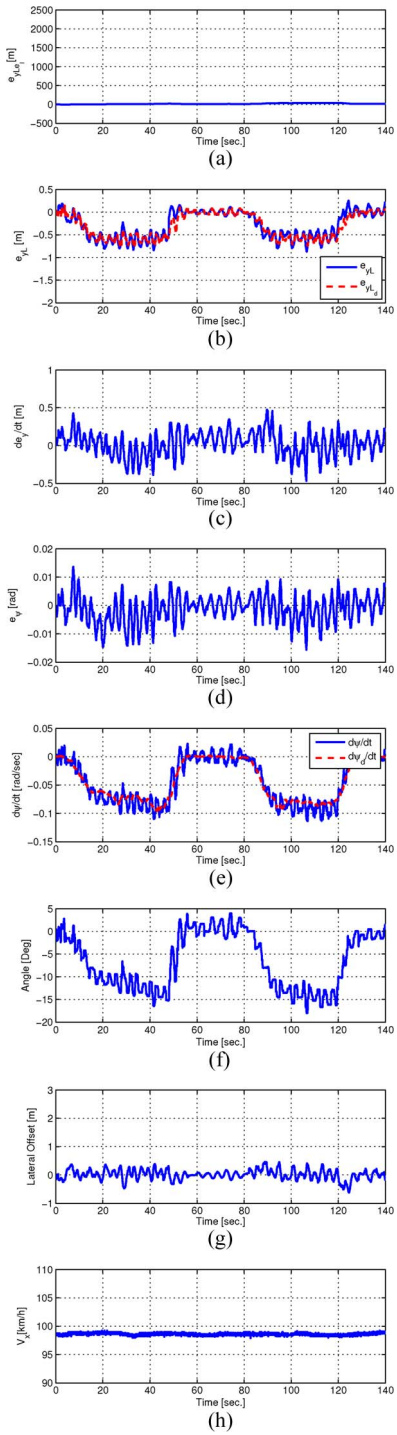

Fig. 13. Lane-keeping control performance of case A.3 (multirate and without an integrator). (a) e_{yLe_I}. (b) e_{yL} and $e_{yL_d}d$. (c) $\dot{e}_y$. (d) e_ψ. (e) $\dot{\psi}$ and $\dot{\psi}_d$. (f) Steering wheel angle. (g) e_y. (h) V_x.

the straight line $g(x)$ of $\overline{P_{k+1}Q_{k+1}}$ and the curve of $f_L(x)$ can be obtained by solving the following:

$$c_0 + c_1 \cdot x + c_2 \cdot x^2 + c_3 \cdot x^3 = m \cdot x + b. \tag{32}$$

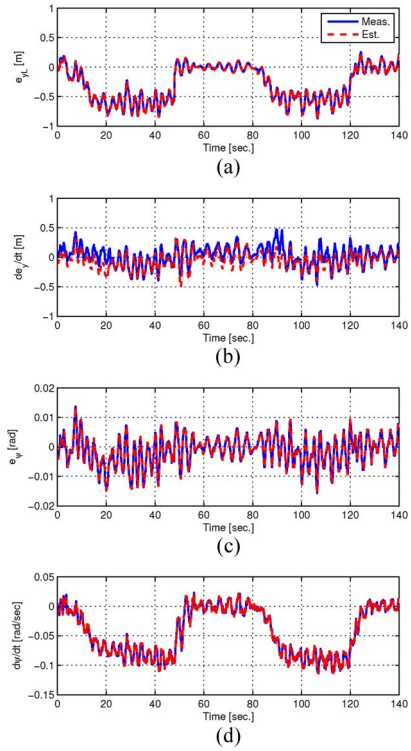

Fig. 14. State estimation performance of case A.3 (multirate and without an integrator). (a) e_{yL}. (b) $\dot{e}_y$. (c) e_ψ. (d) $\dot{\psi}$.

The horizontal coordinate of point Q_{k+1} is obtained by solving (32) using the secant method [40]. Let us define the coordinates of point $Q_{k+1}(\hat{x}_Q(k+1,0), f_L(\hat{x}_Q(k+1,0)))$. Finally, we can obtain $\hat{c}_0(k+1,0)$, which is the Euclidean distance between the two points P_{k+1} and Q_{k+1} such as (33), shown at the bottom of the page.

2) Heading Angle Estimation $\hat{c}_1$: As shown in Fig. 7, the heading angle $\hat{c}_1$ at time $k+1$ is defined by the angle between two tangent lines: the tangent line of the trajectory of the vehicle's c.g. and the tangent line of the trajectory of the lane. To get the angle between the two tangent lines, we first calculate the slopes of the tangent lines at points P_{k+1} and Q_{k+1}. In Fig. 7, we can calculate the values of $\theta_1(k+1,0)$ and $\theta_2(k+1,0)$ by

$$\begin{aligned}\tan\left(\theta_1(k+1,0)\right) &= \frac{df_v(x)}{dx}\Big|_{x=\hat{x}(k+1,0)} \\ \tan\left(\theta_2(k+1,0)\right) &= \frac{df_L(x)}{dx}\Big|_{x=\hat{x}_Q(k+1,0)}.\end{aligned} \tag{34}$$

Then, the difference between $\theta_1(k+1,0)$ and $\theta_2(k+1,0)$, i.e., $\hat{c}_1(k+1,0)$, is obtained by

$$\begin{aligned}\tan\left(\hat{c}_1(k+1,0)\right) &= \tan\left(\theta_1(k+1,0) - \theta_2(k+1,0)\right) \\ &= \frac{m_1 - m_2}{1 + m_1 m_2}\end{aligned} \tag{35}$$

$$\hat{c_0}(k+1,0) = \operatorname{sgn}\left(f_L\left(\hat{x}_Q(k+1,0)\right)\right)\sqrt{\left(\hat{x}_Q(k+1,0) - \hat{x}(k+1,0)\right)^2 + \left(f_L\left(\hat{x}_Q(k+1,0)\right) - f_v\left(\hat{x}(k+1,0)\right)\right)^2} \tag{33}$$

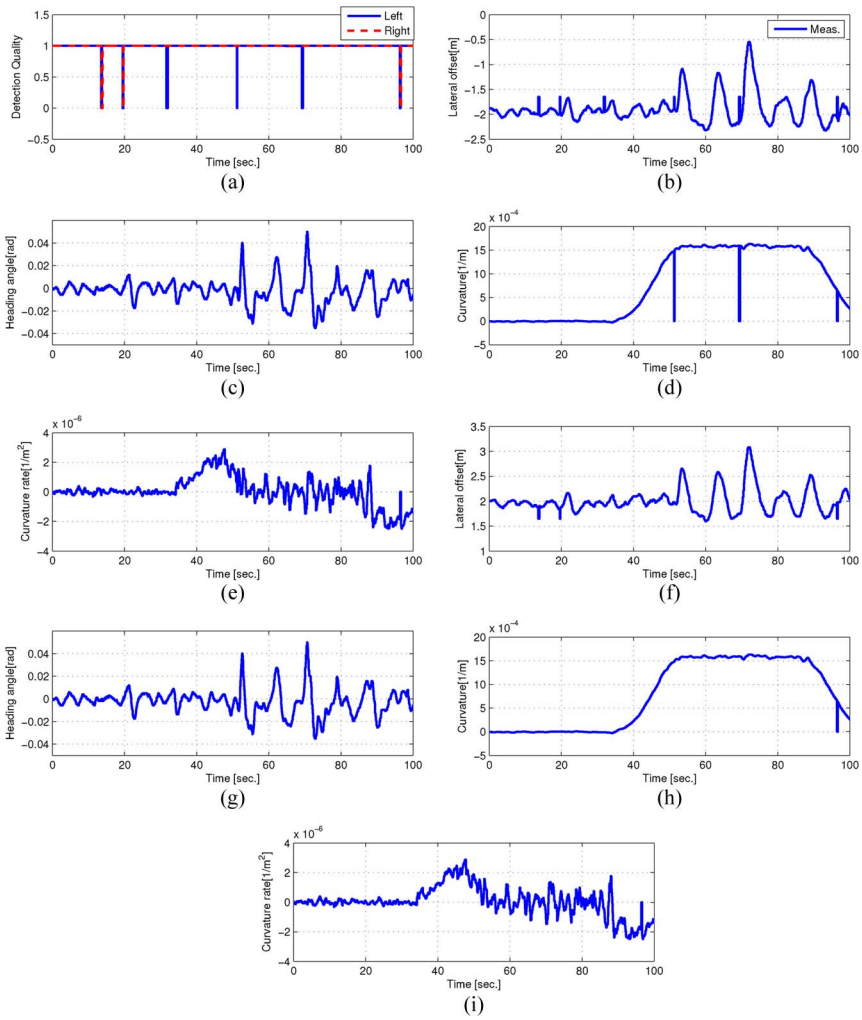

Fig. 15. Lane detection performance of case B.1 (without predictive virtual lane). (a) Detection status. (b) Left lane's lateral offset c_{L_0}. (c) Left lane's heading angle c_{L_1}. (d) Left lane's curvature c_{L_2}. (e) Left lane's curvature rate c_{L_3}. (f) Right lane's lateral offset c_{R_0}. (g) Right lane's heading angle c_{R_1}. (h) Right lane's curvature c_{R_2}. (i) Right lane's curvature rate c_{R_3}.

where $m_1 = \tan(\theta_1(k+1,0))$ and $m_2 = \tan(\theta_2(k+1,0))$. Finally, since $\hat{c}_1(k+1,0)$ is less than 1°, we can approximate it with

$$\hat{c}_1(k+1,0) = \tan^{-1}\left(\frac{m_1 - m_2}{1 + m_1 m_2}\right) \simeq \frac{m_1 - m_2}{1 + m_1 m_2}. \quad (36)$$

3) Curvature and Curvature Rate Estimation $\hat{c}_2$ and $\hat{c}_3$: The estimated curvature $\hat{c}_2$ and curvature rate $\hat{c}_3$ at time $k+1$ are defined as a polynomial with respect to the longitudinal distance x. In the lane polynomial (7), $d^2 f_L(x)/dx^2 = 2c_2 + 6c_3 x$. In the present vehicle's position, x is zero based on the local coordinate of the vehicle so that $d^2 f_L(x)/dx^2|_{x=0} = 2c_2$. Thus, we get the curvature and the curvature rate by (7) at point P_{k+1}, i.e., the next vehicle's position

$$\begin{aligned} 2\hat{c}_2(k+1,0) &= \frac{d^2 f_L(x)}{dx^2}|_{x=\hat{x}(k+1,0)} \\ &= 2c_2(k,0) + 6c_3(k,0)\hat{x}(k+1,0) \end{aligned} \quad (37)$$

and $\hat{c}_3$ is approximated by

$$\hat{c}_3(k+1,0) = \frac{\hat{c}_2(k+1,0) - c_2(k,0)}{\kappa}. \quad (38)$$

Here, κ is a tuning parameter determined by the vehicle speed. The value of κ is influenced by discrete-time approximation and sampling time of the sensor.

Remark 1: The coefficients of the lane polynomial at $k+1$ can be obtained from vehicle and lane data from the camera sensor at time k using the proposed methods in (33) and (36)–(38). If, for several samples, obtaining lane data from the camera results in failure, the virtual lane can be generated from the lane data predicted from the proposed method. For example, the coefficients of the lane polynomial at $k+2$ can be obtained from the vehicle and predicted lane data at time $k+1$ using the proposed method. The performance of the proposed method will be shown in Section V.

V. Experiment Results

The plant to be controlled consists of a Tucson made by Hyundai Motors with a vision system, a yaw rate sensor, and a wheel speed sensor, as shown in Fig. 8. The camera sensor was mounted on the front window shield, the yaw rate sensor was mounted at the c.g. of the vehicle, and the wheel speed sensors were mounted on each wheels. The camera sensor was updated

every 70 ms, whereas the vehicle's motion sensor was updated every 10 ms. The sampling time of the whole system was 10 ms. In this paper, the control gains were designed with the vehicle speed of 80 km/h. The control performance with the gains were experimentally validated for up to 160 km/h on a curved road whose radius was 360 m, but the experimental results at a speed of 27.5 m/s (99 km/h) were included in the paper. We observed that there was no significant degradation of performance for the speed range of 80–160 km/h even on the curved road. Additionally, either feedforward control or integral control could be used to reduce the lateral offset on the curved road.

The experimental tests were performed at the High Speed Circuit of Korea Automobile Testing & Research Institute (KATRI, http://eng.ts2020.kr/) shown in Fig. 9. The specifications of High Speed Circuit are as follows.

- Total length: 5040 m.
- width: 21.2–25.7 m (four lanes).
- Line configuration.
  - — straight line section 967 m × 2;
  - — relief section 411 × 4;
  - — Curve line section 731 × 2;
- Curve radius: 360 m.
- Maximum angle: 42°.
- Maximum speed: 250 km/h (designed speed of 180 km/h).

When the vehicle was running on the High Speed Circuit, the longitudinal velocity was set to between 20 and 35 m/s.

A. *Lane-Keeping Control Performance*

Here, the experiments were tested to validate the lane-keeping control performance of the proposed method during normal operation of the camera sensor. To evaluate the effects of the multirate control and the lateral offset integral term on the lane-keeping control, three cases were tested as follows:

- Case A.1: single-rate lane-keeping control without integrator;
- Case A.2: multirate lane-keeping control without integrator;
- Case A.3: multirate lane-keeping control with integrator.

For cases A.1 and A.2, the intervals of the curved road were from 0 to 60 s and from 90 to 140 s. For case A.3, the intervals of the curved road were from 0 to 60 s and from 80 to 130 s. In other intervals, a straight road was used for all cases. The lane-keeping control performances of cases A.1 and A.2 are shown in Figs. 10 and 11. In both cases A.1 and A.2, the lane-keeping control performances were good on the straight road; therefore, $\mathbf{e}$ was kept near zero. However, the performances on the curved road were poor in comparison to the straight road since the disturbance term $\mathbf{w}$ in (13) increased on the curved road. Thus, the offset error was observed in all states of $\mathbf{e}$. Furthermore, e_{yLe_I} rapidly increased as long as the vehicles were on the curved road due to the absence of the integrator. Fig. 12 shows the yaw rate of cases A.1 and A.2 for comparison. In case A.1, since the single-rate control was used, the lateral dynamics were controlled at the slow rate of the camera sensor. Thus, the relatively large ripple in case A.1 appeared in the yaw rate in comparison with that in case A.2. Although the large ripple in the yaw rate could not affect the other states since the lateral dynamics are in the form of a low-pass filter, it was a main cause of the driver's uncomfortable feeling [21]. On the other hand, using the multirate control resulted in the reduction of the ripple of the yaw rate in case A.2 in comparison with that in case A.1. The lane-keeping control performance of case A.3 is shown in Fig. 13. On the straight road, the lane-keeping control performances of all cases were similar. In contrast, the

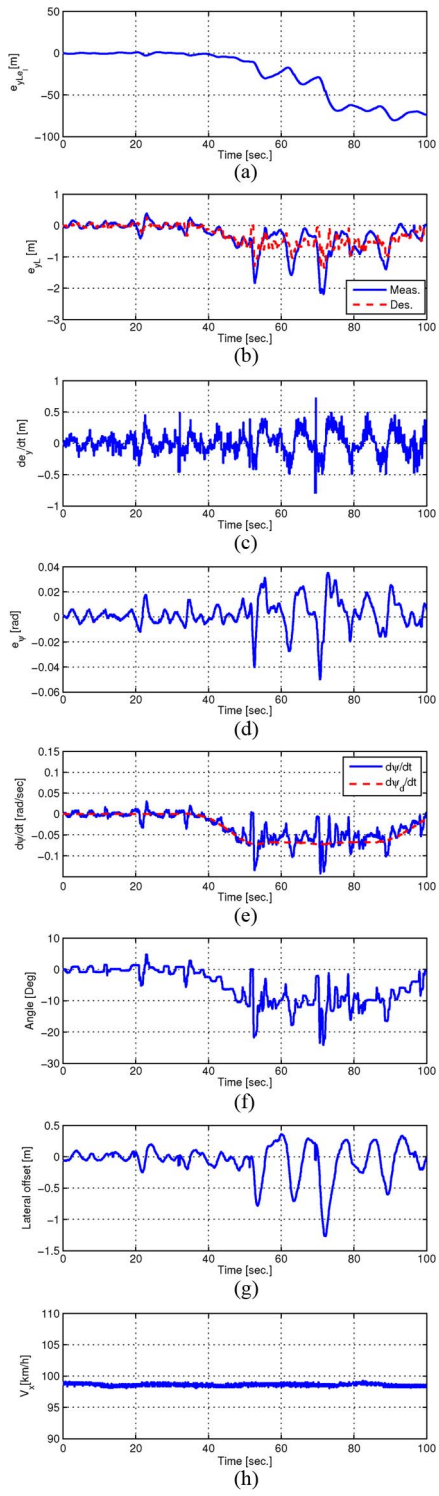

Fig. 16. Lane-keeping performance of case B.1 (without predictive virtual lane). (a) e_{yLe_I}. (b) e_{yL} and e_{yL_d}. (c) $\dot{e}_y$. (d) e_ψ. (e) $\dot{\psi}$ and $\dot{\psi}_d$. (f) Steering wheel angle. (g) e_y. (h) V_x.

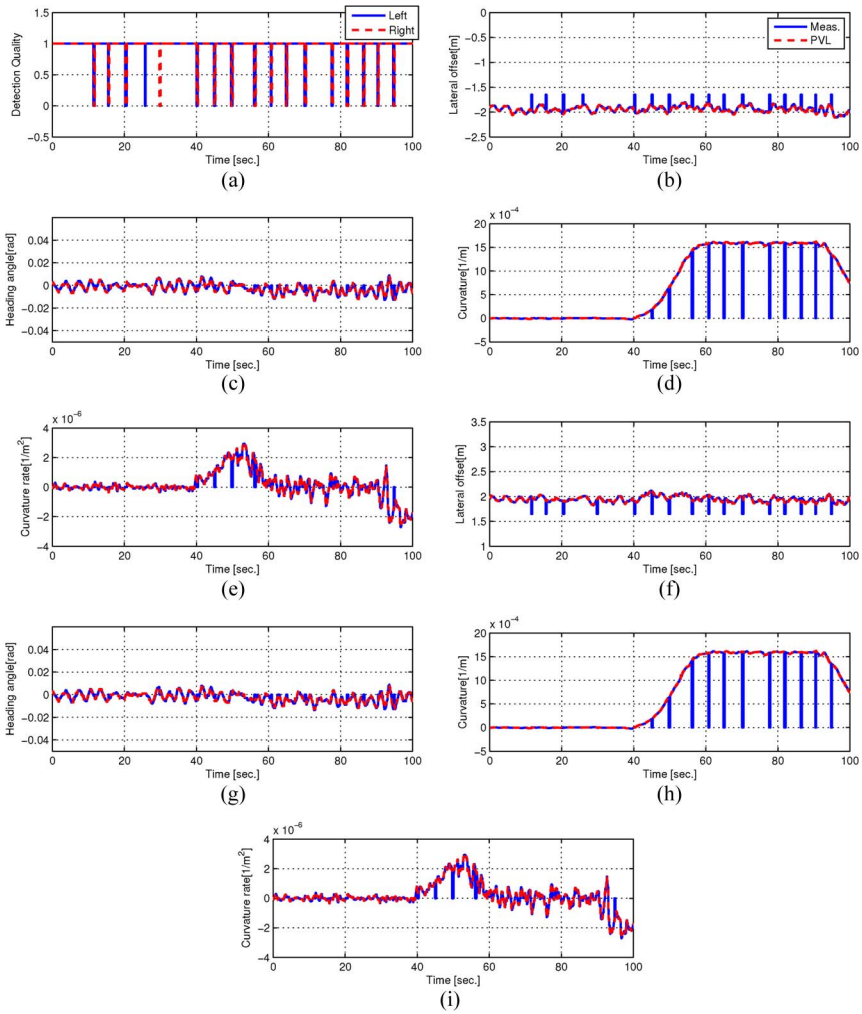

Fig. 17. Lane detection performance of case B.2 (with predictive virtual lane). (a) Detection status. (b) Left lane's lateral offset c_{L_0}. (c) Left lane's heading angle c_{L_1}. (d) Left lane's curvature c_{L_2}. (e) Left lane's curvature rate c_{L_3}. (f) Right lane's lateral offset c_{R_0}. (g) Right lane's heading angle c_{R_1}. (h) Right lane's curvature c_{R_2}. (i) Right lane's curvature rate c_{R_3}.

lane-keeping control performance of case A.3 was superior to those of cases A.1 and A.2 since the integral action suppressed the effect of $\mathbf{w}$ on the curved road. As a result, the lateral offset of case A.3 was less than 20% of those of cases A.1 and A.2, as shown in Figs. 10(g), 11(g), and 13(g). Fig. 14 shows the estimation performance of case A.3. The solid red lines represent the states measured by the camera and IMU sensors, and the blue dashed lines indicate the states estimated by the multirate KF. It is observed that the estimated states tracked the actual states well.

B. Lane-Keeping Control Performance With Predictive Virtual Lane

Here, the experiments were tested to validate the lane-keeping control performance of the proposed predictive virtual lane method when obtaining lane information from the camera sensor failed. To evaluate the effect of the predictive lane-keeping compared with the lane-keeping control, two cases were tested:

- Case B.1: multirate lane-keeping control including an integrator without a predictive virtual lane;
- Case B.2: multirate lane-keeping control including an integrator with a predictive virtual lane.

Fig. 15 shows the lane detection performance of case B.1 for several sampling times on the straight and curved roads under artificial lane detection failure. In Fig. 15(a), the detection status indicates the status of the lane detection for the left and right lanes; "1" indicates success of lane detection, and "0" indicates failure of lane detection. Due to the artificial lane detection failure, several peaking phenomena appeared in the lane detection data corresponding to artificial lane detection failures. The lane-keeping performance of case B.1 is shown in Fig. 16. Several peaking phenomena appeared in the lane keeping corresponding to artificial lane detection failures. Furthermore, as long as the artificial lane detection failures occurred, the lane-keeping performance became worse. The lane detection performance of case B.2 for several sampling times on the straight and curved roads under artificial lane detection failure is shown in Fig. 17. Since we expected that the proposed predictive virtual lane could improve lane detection performance under artificial lane detection failure, the lane detection was set to frequent artificial failure in comparison to case B.1. In Fig. 17(b)–(i), the solid red lines represent the lane measured by the camera

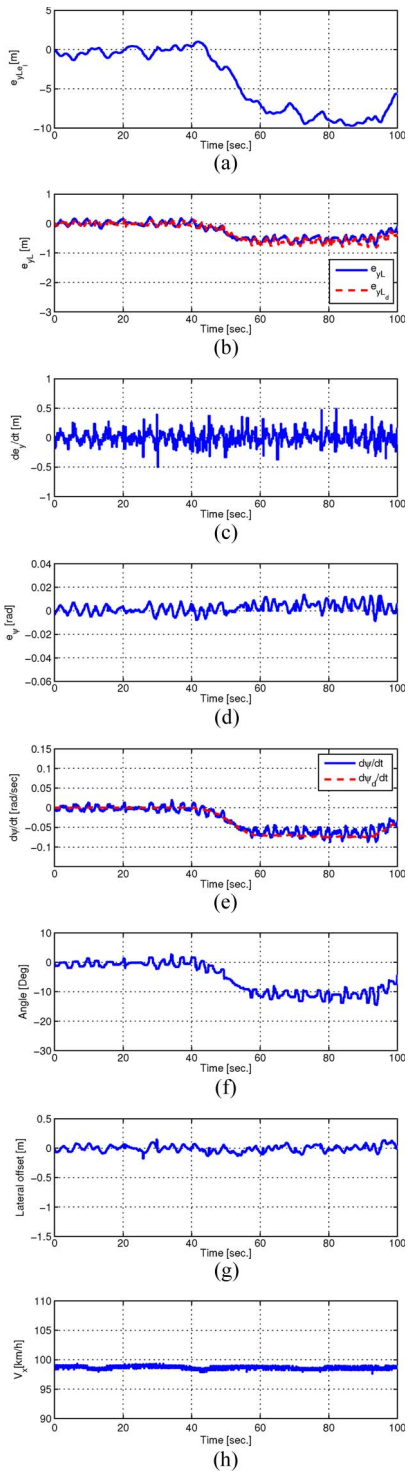

Fig. 18. Lane-keeping performance of case B.2 (with predictive virtual lane). (a) e_{yLe_I}. (b) e_{yL} and e_{yL_d}. (c) $\dot{e}_y$. (d) e_ψ. (e) $\dot{\psi}$ and $\dot{\psi}_d$. (f) Steering wheel angle. (g) e_y. (h) V_x.

sensor, and the dashed blue lines indicate the lane predicted by the proposed method. Although artificial lane detection failure frequently occurred, there was no peaking phenomenon in the lane detection. The lane-keeping performance of case B.2 is shown in Fig. 18. The improved lane detection performance resulted in improved lane-keeping performance. Although the artificial lane detection failures frequently occurred, the lane-keeping performance of case B.2 did not degrade since the predictive virtual lane helped the multirate lane-keeping control normally operating when the lane information was momentarily unavailable. Consequently, the lateral offset of case B.2 was reduced compared with that of case B.1, as shown in Figs. 16(g) and 18(g). Furthermore, oscillations and peaking phenomena disappeared in case B.2. Note that the ripples of the experimental results occurred due to the measurement noise of the camera and IMU sensors.

VI. Conclusion

In this paper, we have proposed a robust multirate control scheme with a predictive virtual lane. The multirate KF was developed to resolve the problems due to slow lane detection by the vision processing system. To improve the lane-keeping performance on the curved road, the linear quadratic state feedback control was designed using the integral of the lateral offset error. We proposed a virtual lane prediction method that adjusts for the momentary failure of lane detection from unexpected problems. The performance of the proposed method was evaluated via experiments. It was observed that the proposed linear quadratic state feedback control with a KF improved the lane-keeping performance and reduced the ripple in the yaw rate. Furthermore, we saw that the proposed control scheme can normally operate by the predictive virtual lane when the lane information is momentarily unavailable.

References

[1] S.-Y. Wang *et al.*, "Trends in road traffic crashes and associated injury and fatality in the People's Republic of China, 1951–1999," *Injury Control Safety Prom.*, vol. 10, no. 1/2, pp. 83–87, Mar.–Jun. 2003.
[2] S. Shladover *et al.*, "Automated vehicle control developements in the path program," *IEEE Trans. Veh. Technol.*, vol. 40, no. 1, pp. 114–130, Feb. 1991.
[3] H. Peng and M. Tomizuka, "Vehicle lateral control for highway automation," in *Proc. Amer. Control Conf.*, 1990, pp. 788–793.
[4] T. Hessburg and M. Tomizuka, "Fuzzy logic control for lateral vehicle guidance," *IEEE Control Syst. Mag.*, vol. 14, no. 4, pp. 55–63, Aug. 1994.
[5] J. K. Hedrick, M. Tomizuka, and P. Varaiya, "Control issues in automated highway systems," *IEEE Control Syst. Mag.*, vol. 50, no. 3, pp. 356–364, Dec. 1994.
[6] S. Patwardhan, H. Tan, and J. Guldner, "A general framework for automatic steering control: System analysis," in *Proc. Amer. Control Conf.*, 1997, pp. 1598–1602.
[7] K. A. Ünyelioğlu, C. Hatipoğlu, and Ü. Özgüner, "Design and stability analysis of a lane following controller," *IEEE Trans. Control Syst. Technol.*, vol. 5, no. 1, pp. 127–134, Jan. 1997.
[8] M. Netto, S. Chaib, and S. Mammar, "Lateral adaptive control for vehicle lane keeping," in *Proc. Amer. Control Conf.*, 2004, pp. 2693–2698.
[9] C. J. Taylor, J. KoSeckd, R. Blasi, and J. Malik, "A comparative study of vision-based lateral control strategies for autonomous highway driving," *Int. J. Robot. Res.*, vol. 18, no. 5, pp. 442–453, May 1999.
[10] S.-J. Wu *et al.*, "The heterogeneous systems integration design and implementation for lane keeping on a vehicle," *IEEE Trans. Intell. Transp. Syst.*, vol. 9, no. 2, pp. 246–263, Jun. 2008.
[11] V. Cerone, M. Milanese, and D. Regruto, "Combined automatic lane-keeping and driver's steering through a 2-DOF control strategy," *IEEE Trans. Control Syst. Technol.*, vol. 17, no. 1, pp. 135–142, Jan. 2009.
[12] L. R. K. Talvala, K. Kritayakirana, and J. C. Gerdes, "Pushing the limits: From lanekeeping to autonomous racing," *Annu. Rev. Control*, vol. 35, no. 1, pp. 137–148, Apr. 2011.
[13] B.-A. Kim, Y. S. Son, S.-H. Lee, and C. C. Chung, "Model predictive control using dual prediction horizons for lateral control," in *Proc. IFAC Intell. Auton. Veh. Symp.*, 2013, pp. 280–285.

[14] K. Kluge and S. Lakshmanan, "A deformable-template approach to lane detection," in *Proc. IEEE Intell. Veh. Symp.*, 1995, pp. 54–59.
[15] Y. Wang, E. K. Teoh, and D. Shen, "Lane detection using B-snake," in *Proc. Int. Conf. Inf. Intell. Syst.*, 1999, pp. 438–443.
[16] Y. He, H. Wang, and B. Zhang, "Color-based road detection in urban traffic scenes," *IEEE Trans. Intell. Transp. Syst.*, vol. 5, no. 4, pp. 309–318, Dec. 2004.
[17] G. F. Franklin, J. D. Powell, and M. L. Workman, *Digital Control of Dynamic Systems*. Reading, MA, USA: Addison-Wesley, 1990.
[18] G. F. Franklin and A. Emami-Nacini, "Design of ripple-free multivariable robust servomechanisms," *IEEE Trans. Autom. Control*, vol. AC-31, no. 7, pp. 661–664, Jul. 1986.
[19] K. L. Moore, S. P. Bhattacharyya, and M. Dahleh, "Capabilities and limitations of multirate control schemes," *Automatica*, vol. 29, no. 3, pp. 941–951, Jul. 1993.
[20] S. H. Lee, "Multirate digital control system design and its application to computer disk drives," *IEEE Trans. Control Syst. Technol.*, vol. 14, no. 1, pp. 124–133, Jan. 2006.
[21] W. Chee and M. Tomizuka, "Lane change maneuver of automobiles for the Intelligent Vehicle and Highway System (IVWS)," in *Proc. Amer. Control Conf.*, 1994, pp. 3586–3587.
[22] C.-Y. Fang, S.-W. Chen, and C.-S. Fuh, "Automatic change detection of driving environments in a vision-based driver assistance system," *IEEE Trans. Neural Netw.*, vol. 14, no. 3, pp. 646–657, May 2003.
[23] H.-Y. Cheng, B.-S. Jeng, P.-T. Tseng, and K.-C. Fan, "Lane detection with moving vehicles in the traffic scenes," *IEEE Trans. Intell. Transp. Syst.*, vol. 7, no. 4, pp. 571–582, Dec. 2006.
[24] J. Melo, A. Naftel, A. Bernardino, and J. Santos-Victor, "Detection and classification of highway lanes using vehicle motion trajectories," *IEEE Trans. Intell. Transp. Syst.*, vol. 7, no. 2, pp. 188–200, Jun. 2006.
[25] Z. Kim, "Robust lane detection and tracking in challenging scenarios," *IEEE Trans. Intell. Transp. Syst.*, vol. 9, no. 1, pp. 16–26, Mar. 2008.
[26] S. Zhou *et al.*, "A novel lane detection based on geometrical model and Gabor filter," in *Proc. IEEE Intell. Veh. Symp.*, 2010, pp. 59–64.
[27] J.-G. Wang, C.-J. Lin, and S.-M. Chen, "Applying fuzzy method to vision based lane detection," *Expert Syst. Appl.*, vol. 37, no. 1, pp. 113–126, Jan. 2010.
[28] R. K. Satzoda, S. Suchitra, and T. Srikanthan, "Robust extraction of lane markings using gradient angle histograms and directional signed edges," in *Proc. IEEE Intell. Veh. Symp.*, 2012, pp. 754–759.
[29] R. Rajamani, H.-S. Tan, B. K. Law, and W.-B. Zhang, "Demonstration of integrated longitudinal and lateral control for the operation of automated vehicles in platoons," *IEEE Trans. Control Syst. Technol.*, vol. 8, no. 4, pp. 695–708, Jul. 2000.
[30] W. Enkelmann, "Video-based driver assistance—From basic functions to applications," *Int. J. Comput. Vis.*, vol. 45, no. 3, pp. 201–221, Dec. 2001.
[31] R. Rajamani, *Vehicle Dynamics and Control*., 2nd ed. New York, NY, USA: Springer-Verlag, 2012.
[32] S. Tsugawa, "Vision-based vehicles in Japan: Machine vision systems and driving control systems," *IEEE Trans. Ind. Electron.*, vol. 41, no. 4, pp. 398–405, Aug. 1994.
[33] C. Hatipoglu, U. Ozguner, and K. A. Redmill, "Automated lane change controller design," *IEEE Trans. Intell. Transp. Syst.*, vol. 4, no. 1, pp. 13–22, Mar. 2003.
[34] J. Ackermann, "Robust car steering by yaw rate control," in *Proc. IEEE Conf. Control*, Dec. 1990, pp. 2033–2034.
[35] E. Bakker, H. Pacejka, and L. Lidner, "A new tire model with an application in vehicle dynamics studies," *Progr. Technol.*, vol. 57, pp. 439–452, 1995.
[36] C. Lin, A. Ulsoy, and D. LeBlanc, "Vehicle dynamics and external disturbance estimation for vehicle path prediction," *IEEE Trans. Control Syst. Technol.*, vol. 8, no. 3, pp. 508–518, May 2000.
[37] F. Ibrahim, "Geometric based path prediction method using moving and stop objects," U.S. Patent 6 643 588, Nov. 4, 2003.
[38] S. Velupillai and L. Guvenc, "Laser scanners for driver-assistance systems in intelligent vehicles," *IEEE Control Syst. Mag.*, vol. 29, no. 2, pp. 17–19, Apr. 2009.
[39] E. Dickmanns, "The development of machine vision for road vehicles in the last decade," in *Proc. IEEE Intell. Veh. Symp.*, 2002, pp. 268–281.
[40] P. Wolfe, "The secant method for simultaneous nonlinear equations," *Commun. ACM*, vol. 2, no. 12, pp. 12–13, Dec. 1959.
[41] S.-H. Lee, Y. O. Lee, B.-A. Kim, and C. C. Chung, "Proximate model predictive control strategy for autonomous vehicle lateral control," in *Proc. Amer. Control Conf.*, 2012, pp. 3605–3610.

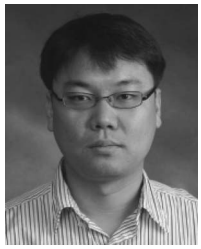

Young Seop Son received the B.S. and M.S. degrees in electronics engineering from Sogang University, Seoul, Korea, in 1997 and 1999, respectively. He is currently working toward the Ph.D. degree with Hanyang University, Seoul.

Since 1999, he has been with the Global R&D Center, MANDO Corporation, Seongnam, Korea. His main research interests include intelligent vehicles, autonomous driving, and robust control.

Mr. Son is a member of the Korea Society of Automotive Engineers; the Institute of Control, Robotics, and Systems; and the Korean Institute of Electrical Engineers.

Wonhee Kim (S'09–M'12) received the B.S. and M.S. degrees in electrical computer engineering and the Ph.D. degree in electrical engineering from Hanyang University, Seoul, Korea, in 2003, 2005, and 2012, respectively.

From 2005 to 2007, he was with Samsung Electronics Company, Korea. In 2012, he was with the Power and Industrial Systems R&D Center, Hyosung Corporation, Korea. In 2013, he was a Postdoctoral Researcher with the Institute of Nano Science and Technology, Hanyang University, and a Visiting Scholar with the Department of Mechanical Engineering, University of California, Berkeley, CA, USA. He is currently an Assistant Professor with the Department of Electrical Engineering, Dong-A University, Busan, Korea. His current research interests include nonlinear control, nonlinear observers, and their industrial applications.

Seung-Hi Lee received the B.S. degree in mechanical engineering from Korea University, Seoul, Korea, in 1985; the M.S. degree in mechanical engineering from Seoul National University in 1987; and the Ph.D. degree in mechanical engineering and applied mechanics from the University of Michigan, Ann Arbor, MI, USA, in 1993.

From 1988 to 1989, he was a Research Scientist with the Korea Institute of Science and Technology. Since 1994, he had been with Samsung Advanced Institute of Technology, Korea, where he was a Team Leader, responsible for advanced servomechanical systems. Since 2009, he has been with Hanyang University, Seoul, as a Research Professor, where he is also teaching advanced control systems. His research interests include robust sampled-data feedback control of uncertain systems and applications to information storage, automotive, electromechanical, and manufacturing systems.

Dr. Lee has served as a member of the Board of Editors of the *International Journal of Control, Automation, and Systems*.

Chung Choo Chung (S'91–M'93) received the B.S. and M.S. degrees in electrical engineering from Seoul National University, Seoul, Korea, and the Ph.D. degree in electrical and computer engineering from the University of Southern California, Los Angeles, CA, USA.

From 1994 to 1997, he was with Samsung Advanced Institute of Technology, Korea. Since 1997, he has been with Hanyang University, Seoul, Korea.

Dr. Chung served as an Associate Editor for the *Asian Journal of Control* from 2000 to 2002 and as an Editor for the *International Journal of Control, Automation, and Systems* from 2003 to 2005. He was a Guest Editor for the special issue on advanced servo control for emerging data storage systems of the IEEE TRANSACTIONS ON CONTROL SYSTEM TECHNOLOGIES (IEEE TCST). He was an Associate Editor for the 2003 IEEE Conference on Decision and Control and an Associate Editor and the Cochair of Publicity for the International Federation of Automatic Control World Congress, Korea, in 2008. He served as a program committee member for the American Society of Mechanical Engineers International Conference on Information Storage and Processing Systems in 2011. He is currently an Associate Editor for TCST, as well as a Program Cochair of the 2015 IEEE Intelligent Vehicles Symposium.